# The Thinnest Molecular Separation Sheet by Graphene Gates of Single-Walled Carbon Nanohorns

**Tomonori Ohba***

Graduate School of Science, Chiba University, 1-33 Yayoi, Inage, Chiba, Chiba 263-8522, Japan

**ABSTRACT** Graphene is possibly the thinnest membrane that could be used as a molecular separation gate. Several techniques including absorption, cryogenic distillation, adsorption, and membrane separation have been adopted for constructing separation systems. Molecular separation using graphene as the membrane has been studied because large area synthesis of graphene is possible by chemical vapor deposition. Control of the gate sizes is necessary to achieve high separation performances in graphene membranes. The separation of molecules and ions using graphene and graphene oxide layers could be achieved by the intrinsic defects and defect donation of graphene. However, the controllability of the graphene gates is still under debate because gate size control at the picometer level is inevitable for the fabrication of the thinnest graphene membranes. In this paper, the controlled gate size in the graphene sheets in single-walled carbon nanohorns (NHs) is studied and the molecular separation ability of the graphene sheets is assessed by molecular probing with $CO_2$, $O_2$, $N_2$, $CH_4$, and $SF_6$. Graphene sheets in NHs with different sized gates of 310, 370, and >500 pm were prepared and assessed by molecular probing. The 310 pm-gates in the graphene sheets could separate the molecules tested, whereas weak separation properties were observed for 370 pm-gates. The amount of $CO_2$ that penetrated the 310 pm-gates was more than 35 times larger than that of $CH_4$. These results were supported by molecular dynamics simulations of the penetration of molecules through 300, 400, and 700 pm-gates in graphene sheets. Therefore, a gas separation membrane using a 340-pm-thick graphene sheet has high potential. These findings provide unambiguous evidence of the importance of graphene gates on the picometer level. Control of the gates is the primary challenge for high-performance separation membranes made of graphene.

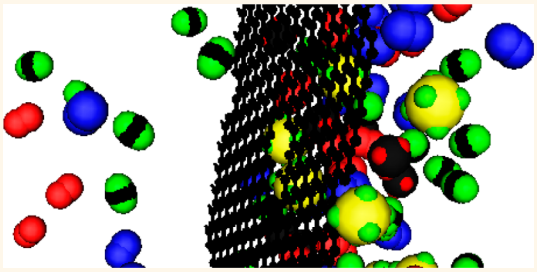

**KEYWORDS:** transport properties · surface science · separation science · molecular modeling · green chemistry · molecular gates · picostructures

The separation of $CO_2$ and $CH_4$ has been increasingly studied.[1−5] Adsorption techniques using porous materials such as zeolites, porous carbons, and metal organic frameworks have shown that the selectivity of $CO_2$ over $CH_4$ is 1−7.[6−8] Selectivity of 20−90 has been reported in membrane separation systems that use organic polymers.[9−11] Basu and co-workers reviewed the separation ability of biogas using such membranes.[11] Graphene is a type of ultrathin organic membrane that has a thickness of 340 pm. Graphene functionalization by edge and molecular gate inclusions, metal insertion, and atomic substitution are some of the most important methods for developing nanotechnologies as well as the synthesis of graphene.[12−19] Jiang and co-workers performed calculations using density functional theory and proposed that molecular gates in graphene can separate $H_2$ and $CH_4$.[20] Kim and co-workers fabricated multilayered graphene and graphene oxide sheets with the ability to separate gases.[21] Graphene layers and graphene oxide layers on polymer membranes have exceeded the upper limit of the molecular selectivity of polymer only membranes. O'Hern and co-workers demonstrated selective ion transport through graphene materials.[22,23] Hence, an ultrathin graphene membrane with high separation ability is important for the future of nanotechnology.

Single-walled carbon nanohorns (NHs) consist of rolled-up graphene, where the graphene sheet that makes up the NH separates the internal and external nanospaces.[24−26] Thus, the separation ability of graphene could be assessed by adsorbing

* Address correspondence to ohba@pchem2.s.chiba-u.ac.jp.

Received for review July 27, 2014 and accepted October 20, 2014.

**Published online October 27, 2014**
**10.1021/nn504162s**

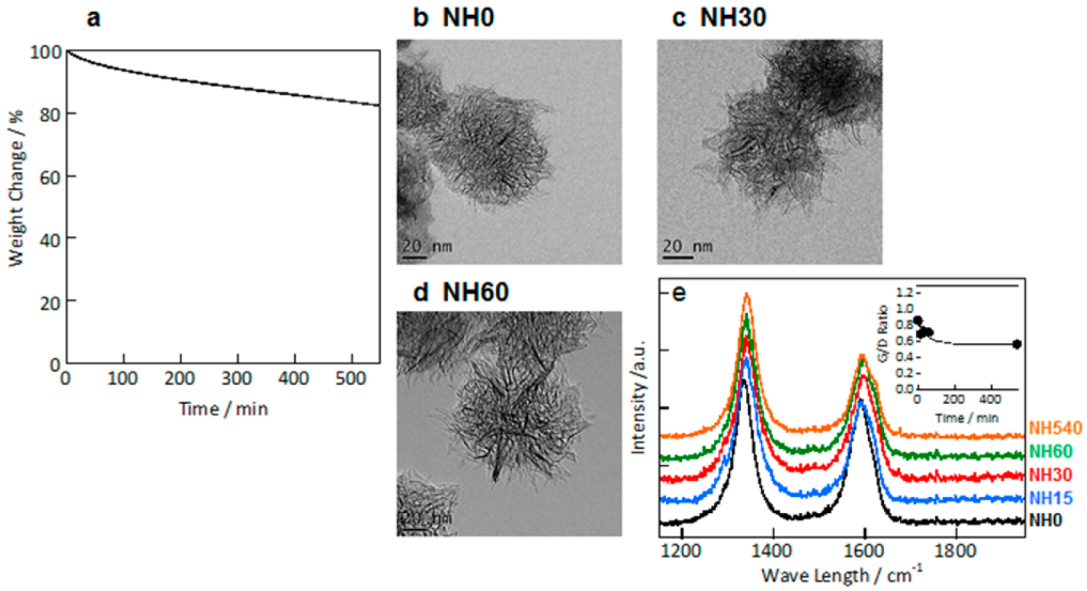


**Figure 1. Maintenance of the NH structure by applying a heat treatment in an $O_2$ atmosphere. (a) Weight changes of the NHs with time in an $O_2$ atmosphere at 673 K. (b–d) Transmission electron microscope (TEM) images of NH0 (b), NH30 (c), and NH60 (d). (e) Raman spectra, excited at 532 nm, for the NHs and the ratio of the G band over the D band as a function of the heating time in the inset.**

molecules into the internal nanospaces. Controlled oxidation of the NHs can produce molecular gates in the graphene sheets in the NHs.[27] In this study, the selective penetrations of $CO_2$, $O_2$, $N_2$, $CH_4$, and $SF_6$ through the molecular gates in the graphene sheets in partially oxidized NHs are evaluated.

## RESULTS AND DISCUSSION

The principal structures of the NHs were maintained after partial oxidation, even though molecular gates had opened (Figure 1). The samples were named as follows: NH0, NH15, NH30, NH60, and NH540, according to the oxidation time, where NH*x* indicates that the NH was oxidized for *x* min at 673 K in an $O_2$ atmosphere. The weight changes of NH0 under an $O_2$ atmosphere at 673 K correspond with the condition of partial oxidation. The weight of NH0 slightly decreased by heating to 673 K in an $O_2$ atmosphere, as shown in Figure 1a, caused by partial oxidation of the NHs. The weight losses, caused by partial oxidation for 15, 30, and 60 min correspond to 2%, 3%, and 4% of the NH0 weight. The transmission electron microscope (TEM) images in Figure 1b–d show that the NH particles are 40–50 nm in length and radiate in all directions from the core in what is commonly referred to as a dahlia-flower-like structure. The diameter of the closed NH assembly is approximately 100 nm. All of the NH particles maintained their structure after they had been partially oxidized, which is also supported by the Raman spectroscopy measurements in Figure 1e. The molecular penetration through the nanogates in the graphene sheets is demonstrated and evaluated by the differences in the amounts of adsorption in the oxidized NHs and NH0, as shown in Supporting Information Figure S1. The penetration of $SF_6$, which was the largest molecule used in this study, was not restricted by the gates in NH60, because the amounts of adsorption for NH60 and NH540 approximately coincided with each other. Therefore, NH60 had large enough gates for $O_2$, $CO_2$, $N_2$, and $CH_4$ to penetrate through. We presumed that NH0 did not have any gates. There was an obvious difference between the oxidized NHs and NH0 for the adsorption isotherms of $N_2$ at 77 K. This means that the graphene gates in the internal nanospaces were fabricated in oxidized NHs and have the ability to separate different molecules. The nanospace volumes for NH0, NH15, NH30, and NH60 were 0.14, 0.21, 0.58, and 0.58 mL $g^{-1}$, respectively, evaluated by $\alpha_S$-analysis of the $N_2$ adsorption isotherms. The nanospace volumes for NH30 and NH60 were similar to each other despite the different oxidation rates, indicating that the gate sizes were larger than the molecular size of $N_2$ for oxidation times longer than 30 min. As the difference in the nanospace volumes between the oxidized NHs and NH0 is attributed to the adsorption in the internal nanospaces, the total volume of the nanospaces for the internal and external nanospaces was 0.44 and 0.14 mL $g^{-1}$, respectively, evaluated from the nanospace volumes of NH60 or NH30 and NH0. About 16% of the internal nanospaces in NH15 was available for the adsorption of $N_2$ at 77 K owing to the extremely narrow molecular gates. The amounts of $CO_2$ and $CH_4$ that penetrated the graphene sheets decreased with a decreasing oxidization time, *i.e.*, a decreasing gate size, shown in Figure 2b,e, whereas the penetrations of $O_2$ through the graphene sheets (Figure 2a) were all similar to each other. Only $SF_6$ could penetrate through the NH60 gates (Figure 2f).

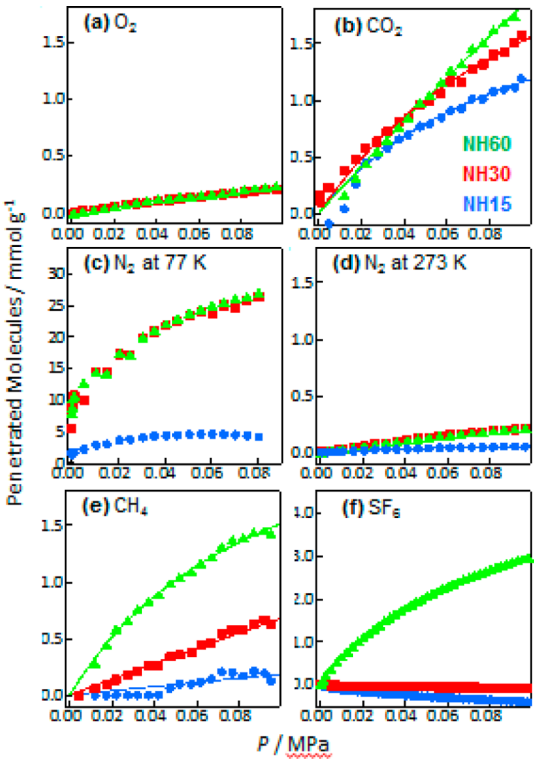


**Figure 2. Molecular penetrations through the graphene gates in NHs. The amounts of $O_2$ at 273 K (a), $CO_2$ at 273 K (b), $N_2$ at 77 K (c), $N_2$ at 273 K (d), $CH_4$ at 273 K (e), and $SF_6$ at 303 K (f) that penetrated through the graphene sheets were obtained by subtracting the adsorption isotherms on the oxidized NHs from those on the NH0. The penetration of $SF_6$ through the gates in NH60 was significant, but no $SF_6$ penetrated through the gates in NH15 and NH30. The amounts of $O_2$ at 273 K that penetrated through NH15, NH30, and NH60 were all similar to each other. However, the amounts of other molecules that penetrated through the gates were different for the different NHs. This indicated that the graphene gates in the NHs efficiently separated $CO_2$, $CH_4$, and $N_2$ by varying the sizes of the gates.**

$SF_6$ penetrations through the NH15 and NH30 gates were decreased with increasing pressure. This was caused by significant buoyancy of both NHs in $SF_6$ adsorption, because $SF_6$ rarely penetrates through the NH15 and NH30 gates, as mentioned later. $N_2$ was prevented from penetrating through NH15 (Figure 2c,d). $CH_4$ penetration through the NH15 gates was severely restricted below 0.04 MPa, although the NH15 gates slightly permitted $CH_4$ penetration above 0.04 MPa. The gate opening by increasing pressure is a result of graphene flexibility. The tendencies of $N_2$ adsorption isotherms at 77 and 273 K in Figure 2c,d resemble each other; penetrated molecular numbers for the NH30 and NH60 were similar at each temperature, but those for the NH15 were rather smaller than the others. Thus, molecules were separated by gate size, not by blocking.

As molecular penetration occurred when the molecular size was smaller than the size of the graphene gates, the gate size could be determined from the size of the molecules that penetrated the sheets. Therefore, NH30 had larger gates than the molecular sizes of $O_2$

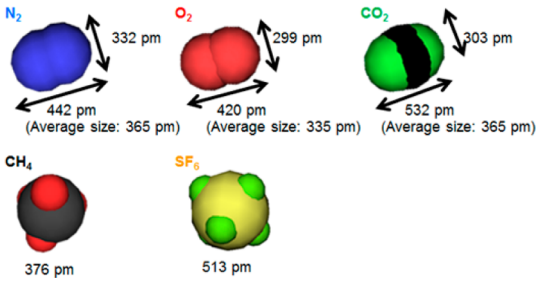


**Figure 3. Molecular sizes of $N_2$, $O_2$, $CO_2$, $CH_4$, and $SF_6$. The molecular sizes were evaluated from the collision diameter of the Lennard-Jones potential. The average size is defined as $2 \times (a^2c)^{1/3}$, where $a$ and $c$ are the short and long radii of the spheroids, respectively.**

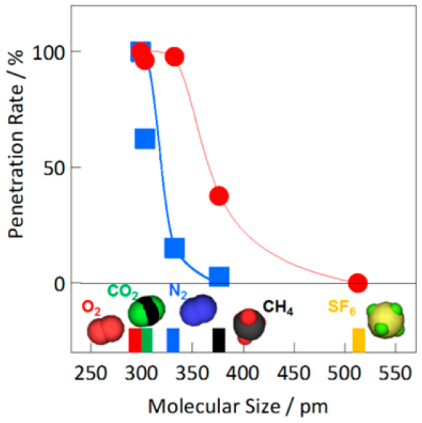


**Figure 4. Molecular penetration rates in NH15 (blue curve) and NH30 (red curve) as a function of the molecular size. The molecular sizes are defined as the shorter diameter for a spheroid molecule and the diameter for a spherical molecule. The symbols were obtained from the penetrated molecular rates at 0.08 MPa in Figure 2. The solid curves are the fitting curves, obtained by assuming that the gate sizes had Gaussian distributions.**

(299 pm), $CO_2$ (303 pm), and $N_2$ (332 pm), but slightly smaller gates than the molecular size of $CH_4$ (376 pm). Here the molecular sizes are shown in Figure 3.[28−30] Thus, the size of the gates in the NH30 sample was in the range of 332−376 pm. $O_2$ molecules also penetrated the gates in NH15, while the penetration of $CO_2$ in NH15 decreased and the penetration of $N_2$ and $CH_4$ was rarely observed. This indicated that the size of the gates in NH15 was between the $CO_2$ and $N_2$ molecular sizes, *i.e.*, between 303 and 332 pm. Figure 4 shows the molecular penetration rates for NH15 and NH30 as a function of the molecular size, evaluated by the amount of each molecule that penetrated the samples (shown in Figure 2). Here $N_2$ penetration was assessed from $N_2$ adsorptions at 77 K, because $N_2$ adsorptions at 77 K gave more accurate penetration rates than those at 273 K. Gaussian distributions of the gate sizes (Figure 5a) were obtained by fitting the molecular penetration rates under the assumption that a molecule could penetrate a gate larger than its molecular size. NH15 and NH30 had graphene gate sizes of $310 \pm 20$ and $370 \pm 20$ pm, respectively. Therefore, the graphene

gates in NH15 permitted $O_2$ and $CO_2$ to penetrate, but prevented $N_2$ and $CH_4$ from penetrating through, as shown in Figure 5b. In contrast, the graphene gates in NH30 permitted $O_2$, $CO_2$, and $N_2$ to penetrate, but prevented $CH_4$ from penetrating through (Figure 5c). Therefore, these graphene gates could separate $O_2$, $CO_2$, $N_2$, and $CH_4$, despite having the thickness of a single graphene sheet (340 pm thick). Selective penetration through the graphene gates was evaluated for $CO_2$ and $CH_4$, as shown in Figure 5d. Molecular selectivity of $CO_2$ over $CH_4$ was defined as the ratio of the number of $CO_2$ molecules divided by the number of $CH_4$ molecules that could penetrate through the graphene gates in the NHs, at a constant pressure. The graphene gates in NH15 had extremely high separation ability, whereas both $CO_2$ and $CH_4$ could penetrate through the gates in NH60. The selectivity of the graphene gates in NH60 was nearly 1; that is, the amounts of $CO_2$ and $CH_4$ that could penetrate were equivalent because the gates were large enough for both molecules to pass through. NH30 had a relatively high selectivity of 2−3 because the average gate size in NH30 was 370 pm, which is between the molecular sizes of $CO_2$ and $CH_4$ (303 and 376 pm, respectively). Surprisingly, a significant selectivity from 18 to more than 35 was observed for NH15. As the average gate size for NH15 was 310 pm, $CH_4$ was close to the limit of penetration through the gates in NH15, but $CO_2$ could easily penetrate. Studies have shown that the selectivity of $CO_2/CH_4$ is 1−7 for adsorption separation and 20−80 for membrane separation.[1,4,7−10] Separation using graphene gates is much higher than that using an adsorption technique and similar to a membrane technique. However, the membrane separation technique is different from the gate separation technique used in this study. Furthermore, the graphene gates in the NHs separated molecules through 340-pm-thick graphene sheets. The selectivity is extremely high when both the selectivity and thickness are both taken into account.

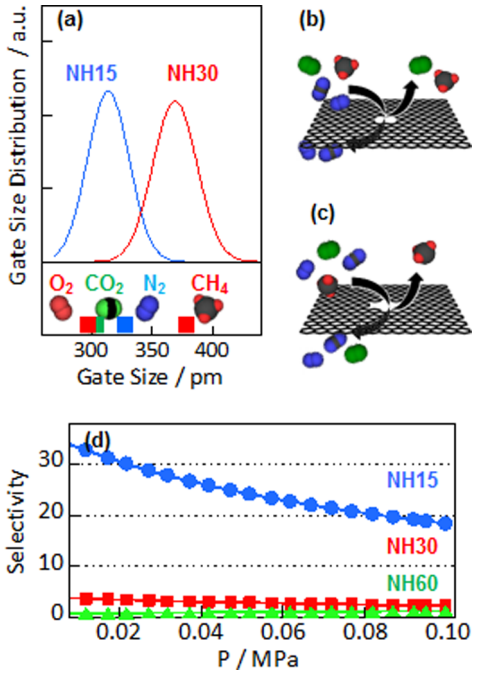


**Figure 5. Molecular separation through the graphene gates in NHs. (a) Gate size distributions for NH15 and NH30. NH15 and NH30 had gates with average diameters of 310 and 370 pm, respectively. (b and c) Schematic diagrams of the penetration of molecules through the graphene gates in NH15 and NH30, respectively. (d) Selectivity of $CO_2$ over $CH_4$ for NH15, NH30, and NH30.**

The penetrations of $N_2$, $O_2$, $CO_2$, $CH_4$, and $SF_6$ through three types of gates in graphene sheets were evaluated with molecular dynamics simulations, as shown in Figure 6. The 300 and 400 pm-gate graphene samples approximately corresponded to the gate sizes of the NH15 and NH30 samples, respectively. The force fields (Figure 7) were obtained from the Lennard-Jones potential functions between the molecules and the graphene sheets. The vertically aligned linear molecules against the graphene walls and spherical molecules were shifted from $z = -2.5$ to 2.5 nm at $x = y = 0$ in the unit cells. The positive and negative forces mean

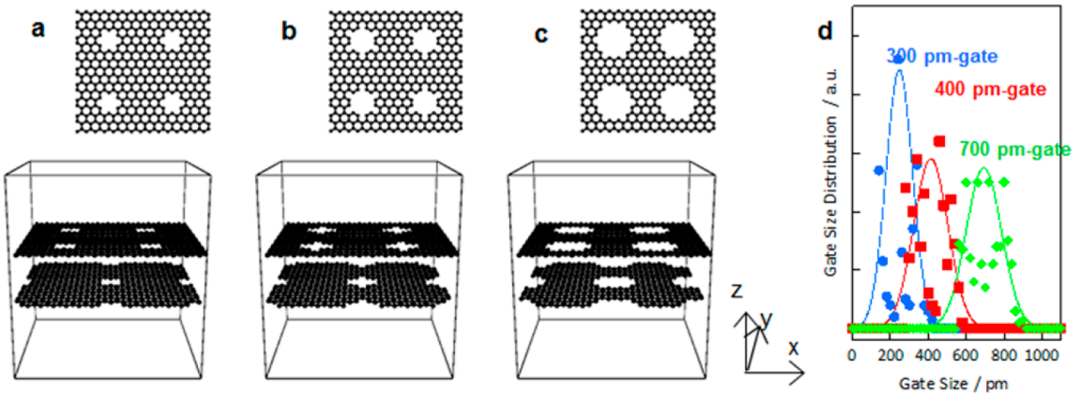


**Figure 6. Setups for the molecular dynamics simulations of the penetrations of molecules through graphene gates. Graphene sheets containing 4 gates with diameters of 300 pm (a), 400 pm (b), and 700 pm (c). (d) Graphene gate size distributions in the three models. The gates were named the 300, 400, and 700 pm-gates, according to their size distributions.**

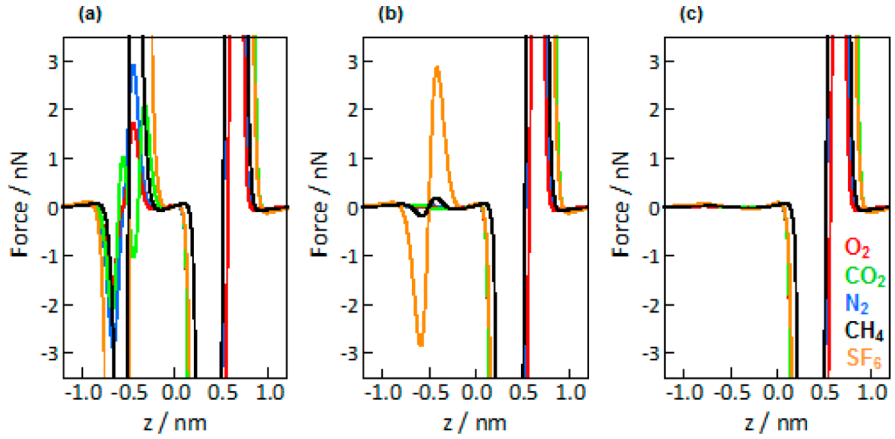


**Figure 7. Force fields of the molecules in the graphene sheets. Graphene sheets with gates 300 (a), 400 (b), and 700 pm (c) in diameter.**

that a molecule receives a force in the positive and negative directions along the *z*-axis, respectively. The force fields of the penetrating molecules showed that the penetration barrier was suppressed with an increasing gate size. The force fields of the molecules evaluated from the Lennard-Jones potential functions indicated that a large potential barrier was observed for the penetration through a 300 pm-gate graphene sheet. In contrast, the barrier was suppressed for the 400 pm-gate graphene sheet, except for $SF_6$. All of the molecules could penetrate through the 700 pm-gate graphene without a considerable energy barrier. The snapshots in Supporting Information Figures S2−S16 show the penetrations of the molecules into the nanospaces between the graphene sheets. The number of molecules that could penetrate the samples was evaluated from these snapshots for 300, 400, and 700 pm-gate graphene samples, as shown in Figure 8a−c. The number of molecules that could pass through the gates was dependent on the size of the gates. All of the molecular species could easily penetrate through the 700 pm-gates, and thus, the graphene gates were open for all of the molecules. The 400 pm-gate graphene layer also permitted the molecules to penetrate through the gates, except for $SF_6$. $CO_2$ and $O_2$ could comparatively penetrate through the 300 pm-gate and $N_2$ molecules somewhat penetrated as well. However, $CH_4$ and $SF_6$ could not pass through the 300 pm-gates. The penetration factor is defined as the rate that molecules penetrate through the gates divided by the number that penetrated through 700 pm-gates, as shown in Supporting Information Figure S17. The decrease in the number of molecules that penetrated the samples was a result of the equivalent gate size and the size of the molecules. The size restriction in the 300 pm-gate model was very strict; the penetration factors of $O_2$, $CO_2$, $N_2$, $CH_4$, and $SF_6$ for the 300 pm-gate were 0.53, 0.68, 0.17, 0.00, and 0.00, respectively. In contrast, the penetration factors of $O_2$, $CO_2$, $N_2$, $CH_4$, and $SF_6$ for the 400 pm-gate were

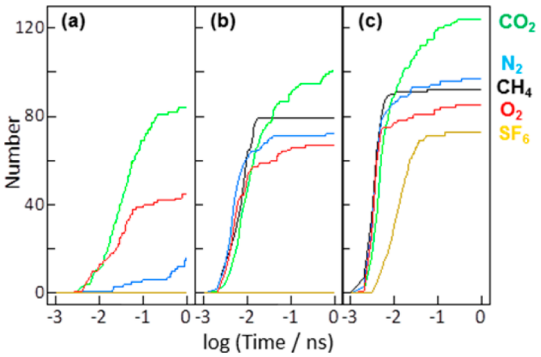


**Figure 8. Simulations of the penetration of molecules through graphene gates. Changes in the number of $O_2$, $CO_2$, $N_2$, $CH_4$, and $SF_6$ molecules that penetrated through the gates using graphene layer models with 300 (a), 400 (b), and 700 pm-gates (c), obtained from the snapshots of the molecular dynamics simulations.**

0.79, 0.81, 0.74, 0.86, and 0.00, respectively. The high penetration factor of $CH_4$ was caused by its strong adsorption potential. Thus, the $CH_4$ and $SF_6$ molecules were strongly repelled by the 300 pm-gates and the $N_2$ molecules also had restricted penetration through the gates.

The simulated selectivity, defined as the ratio between the amounts of different molecules that penetrated the samples, indicated that $CO_2$ and $CH_4$ were completely separated through the 300 pm-gate graphene, as shown in Figure 9. Selectivity is defined as the ratio between the amounts of the different molecules that penetrated the sample. The selectivity of $CO_2$ over $CH_4$ for the 300 pm-gates was significantly high, whereas that for the 400 and 700 pm-gates was nearly one. Thus, $CO_2$ and $CH_4$ were rarely separated for the 400 and 700 pm-gates. The significantly high selectivity of $CO_2$ over $CH_4$ through NH15 and NH30 in the experiments (Figure 5d) was caused by the selective penetration through the 300 pm-gates. A high selectivity of $O_2$ over $N_2$ was also observed with the 300 pm-gate graphene; 13 at 0.01 ns, 6.5 at 0.1 ns and 2.8 at 1 ns. An experimental study on the kinetically driven

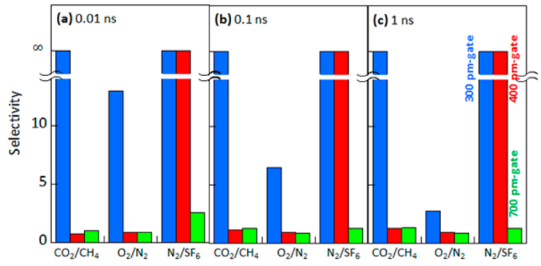


**Figure 9. Selective penetration through the 300, 400, and 700 pm-gates. Selectivity between $CO_2$ and $CH_4$, $O_2$ and $N_2$, and $SF_6$ and $N_2$ through the gates in the graphene sheets at 0.01 (a), 0.1 (b), and 1 ns (c).**

penetration through the graphene gates is necessary to observe the difference between the penetration of $O_2$ and $N_2$. $SF_6$ and $N_2$ were also well separated, even through the 400 pm-gates. This selectivity agrees with the experimental results for the adsorption isotherms of $SF_6$ and $N_2$ in NH15 and NH30.

## CONCLUSION

In conclusion, the penetration of molecules through the gates in graphene sheets in NHs was comprehensively assessed using experiments and molecular dynamics simulations. $CO_2$ and $CH_4$ were well separated through 310 pm-gates in graphene sheets in NHs, demonstrating that a 340-pm-thick graphene sheet can separate $CO_2$ and $CH_4$. Molecular dynamics simulations suggested that such separation could be possible with 300 pm-gates and the dynamic separation of molecules provided higher selectivity. Further studies using dynamical measurements are needed to develop the separation of fluids using graphene membranes.

## METHODS

**Preparation of NHs and Experiments.** Partial oxidation of NHs was conducted to open up gates by heating them in an $O_2$ atmosphere of 100 mL $min^{-1}$ at 673 K for 15, 30, and 60 min. Thermogravimetric curves were measured using the above conditions to evaluate the oxidation rates of the NHs. Transmission electron microscope images using a JEM-2100F instrument (JEOL Co., Tokyo, Japan) at 120 keV and Raman spectroscopy using the 532 nm line of a green laser with an incident power of 0.1 mW (NRS-3100, JASCO, Tokyo, Japan) were performed to evaluate how well the NH structures were maintained when they were partially oxidized. $N_2$ adsorption isotherms at 77 K were measured for the oxidized and as-prepared NHs (called NH0) for comparison using a volumetric apparatus (Autosorb-1; Quantachrome Co., Boynton Beach, FL). The $O_2$, $CH_4$, and $CO_2$ adsorption isotherms were measured at 273 K, and the $SF_6$ adsorption isotherms were measured at 303 K. The NHs were evacuated at 423 K below 10 mPa more than 2 h prior to each adsorption measurement.

**Simulation Procedures.** Molecular dynamics simulations were performed to investigate the penetration of molecules through graphene sheets with different gate sizes of 300, 400, and 700 nm using the leapfrog algorithm with a single time step of 1.0 fs in a canonical ensemble. A temperature range of 320 ± 20 K was maintained using the heat bath coupling method. The molecular coordinates were output for trajectory analysis. A periodic boundary condition was adopted in all three directions ($x$, $y$, and $z$). Two graphene sheets were assumed to be rigid and arranged parallel to each other at distances of 500 pm from the center of the unit cell, that is, at $z = 500$ and $-500$ pm, as shown in Figure 6. Each graphene sheet was composed of 462 carbon atoms. The 200 $N_2$, $O_2$, $CO_2$, $CH_4$, and $SF_6$ molecules were arranged above the top of the graphene sheet and below the bottom graphene sheet in the unit cell that was 3.197 × 3.834 × 4.000 $nm^3$ in size. The molecules were randomly arranged with intermolecular distances more than double their molecular size. The graphene sheets had gate sizes of 250 ± 80, 410 ± 110, and 690 ± 110 pm, which were named the 300, 400, and 700 pm-gates, respectively. The three graphene gate sizes were obtained by removing 12, 24, or 48 carbon molecules. Molecular penetration through the graphene gates in the three models were tested using the molecular models with an integration time of 1.0 ns. Two centered Lennard-Jones-type potential models were used for the $N_2$ and $O_2$ pairwise potential. The collision diameter and interaction potential were $\sigma_N = 332$ pm and $\varepsilon_N/k_B = 36.4$ K for $N_2$, and $\sigma_O = 299$ pm and $\varepsilon_O/k_B = 52.0$ K for $O_2$.[28] The molecular distances between the $N_2$ and $O_2$ molecules were 110 and 120.8 pm, respectively. The three centered Lennard-Jones-type potential model with three partial charges was adopted for the $CO_2$ pairwise potential. The collision diameters and interaction potentials of $CO_2$ were $\sigma_C = 275.3$ pm, $\varepsilon_C/k_B = 29.07$ K, $\sigma_O = 302.9$ pm and $\varepsilon_O/k_B = 83.2$ K.[29] Partial charges of +0.6466 and −0.3233 $e$ were located on the C and O atoms, respectively. The C−O distance was 114.3 pm. The one centered Lennard-Jones-type potentials of $CH_4$ and $SF_6$ were adopted: $\sigma_{CH4} = 375.8$ pm and $\varepsilon_{CH4}/k_B = 148.6$ K for $CH_4$, and $\sigma_{SF6} = 512.8$ pm and $\varepsilon_{SF6}/k_B = 222.1$ K for $SF_6$.[30] A graphene potential model was constructed based on ideal graphite, which has a honeycomb lattice; the C−C distance was 142 pm. The collision diameter and interaction potential were $\sigma_C = 340$ pm and $\varepsilon_C/k_B = 28.0$ K.[31] Ewald summation was applied to the long-range coulomb interactions between the $CO_2$ molecules. The Lorentz−Berthelot mixing rules were applied to calculate the collision diameters and interaction potentials in the Lennard-Jones potential between the molecules with different potential parameters. Weak external forces of 0.1 and −0.1 nN were applied to the molecules at $z < 0$ and >0, respectively, to control the molecular flow at the center of the two graphene sheet.

*Conflict of Interest:* The authors declare no competing financial interest.

*Supporting Information Available:* Adsorption isotherms of $O_2$, $CO_2$, $N_2$, $CH_4$, and $CO_2$, snapshots, and molecular penetration through gates in simulation. This material is available free of charge *via* the Internet at http://pubs.acs.org.

*Acknowledgment.* The author would like to thank Dr. M. Yudasaka from the Nanotube Research Center, Advanced Industrial Science and Technology, Japan and Prof. S. Iijima from Meijo University, Japan for supplying the NHs. The transmission electron microscope observations were conducted at the Center for Analytical Instrumentation, Chiba University. This research was supported by the Japan Society for the Promotion of Science KAKENHI Grant Number 26706001 and Research Fellowships from the Futaba Electronics Memorial Foundation.

## REFERENCES AND NOTES

1. Couck, S.; Denayer, J. F.; Baron, G. V.; Rémy, T.; Gascon, J.; Kapteijn, F. An Amine-Functionalized Mil-53 Metal−Organic Framework with Large Separation Power for $CO_2$ and $CH_4$. *J. Am. Chem. Soc.* **2009**, *131*, 6326–6327.
2. Kapoor, A.; Yang, R. T. Kinetic Separation of Methane—Carbon Dioxide Mixture by Adsorption on Molecular Sieve Carbon. *Chem. Eng. Sci.* **1989**, *44*, 1723–1733.

3. Hernández-Huesca, R.; Díaz, L.; Aguilar-Armenta, G. Adsorption Equilibria and Kinetics of $CO_2$, $CH_4$ and $N_2$ in Natural Zeolites. *Sep. Purif. Technol.* **1999**, *15*, 163–173.
4. Babarao, R.; Hu, Z.; Jiang, J.; Chempath, S.; Sandler, S. I. Storage and Separation of $CO_2$ and $CH_4$ in Silicalite, $C_{168}$ Schwarzite, and Irmof-1: A Comparative Study from Monte Carlo Simulation. *Langmuir* **2007**, *23*, 659–666.
5. Babarao, R.; Jiang, J. Diffusion and Separation of $CO_2$ and $CH_4$ in Silicalite, $C_{168}$ Schwarzite, and Irmof-1: A Comparative Study from Molecular Dynamics Simulation. *Langmuir* **2008**, *24*, 5474–5484.
6. Bae, Y. S.; Mulfort, K. L.; Frost, H.; Ryan, P.; Punnathanam, S.; Broadbelt, L. J.; Hupp, J. T.; Snurr, R. Q. Separation of $CO_2$ from $CH_4$ Using Mixed-Ligand Metal-Organic Frameworks. *Langmuir* **2008**, *24*, 8592–8598.
7. Bastin, L.; Barcia, P. S.; Hurtado, E. J.; Silva, J. A. C.; Rodrigues, A. E.; Chen, B. A Microporous Metal-Organic Framework for Separation of $CO_2/N_2$ and $CO_2/CH_4$ by Fixed-Bed Adsorption. *J. Phys. Chem. C* **2008**, *112*, 1575–1581.
8. Finsy, V.; Ma, L.; Alaerts, L.; De Vos, D. E.; Baron, G. V.; Denayer, J. F. M. Separation of $CO_2/CH_4$ Mixtures with the Mil-53(Al) Metal−Organic Framework. *Microporous Mesoporous Mater.* **2009**, *120*, 221–227.
9. Vu, D. Q.; Koros, W. J.; Miller, S. J. High Pressure $CO_2/CH_4$ Separation Using Carbon Molecular Sieve Hollow Fiber Membranes. *Ind. Eng. Chem. Res.* **2002**, *41*, 367–380.
10. Staudt-Bickel, C.; J. Koros, W. Improvement of $CO_2/CH_4$ Separation Characteristics of Polyimides by Chemical Crosslinking. *J. Membr. Sci.* **1999**, *155*, 145–154.
11. Basu, S.; Khan, A. L.; Cano-Odena, A.; Liu, C.; Vankelecom, I. F. Membrane-Based Technologies for Biogas Separations. *Chem. Soc. Rev.* **2010**, *39*, 750–768.
12. Radovic, L. R.; Bockrath, B. On the Chemical Nature of Graphene Edges: Origin of Stability and Potential for Magnetism in Carbon Materials. *J. Am. Chem. Soc.* **2005**, *127*, 5917–5927.
13. Radovic, L. R. Active Sites in Graphene and the Mechanism of $CO_2$ Formation in Carbon Oxidation. *J. Am. Chem. Soc.* **2009**, *131*, 17166–17175.
14. Ohba, T.; Kanoh, H. Intensive Edge Effects of Nanographenes in Molecular Adsorptions. *J. Phys. Chem. Lett.* **2012**, *3*, 511–516.
15. Xu, C.; Wang, X.; Zhu, J. Graphene−Metal Particle Nanocomposites. *J. Phys. Chem. C* **2008**, *112*, 19841–19845.
16. Ci, L.; Song, L.; Jin, C.; Jariwala, D.; Wu, D.; Li, Y.; Srivastava, A.; Wang, Z. F.; Storr, K.; *et al.* Atomic Layers of Hybridized Boron Nitride and Graphene Domains. *Nat. Mater.* **2010**, *9*, 430–435.
17. Li, X.; Cai, W.; An, J.; Kim, S.; Nah, J.; Yang, D.; Piner, R.; Velamakanni, A.; Jung, I.; *et al.* Large-Area Synthesis of High-Quality and Uniform Graphene Films on Copper Foils. *Science* **2009**, *324*, 1312–1314.
18. Lee, E. J.; Balasubramanian, K.; Weitz, R. T.; Burghard, M.; Kern, K. Contact and Edge Effects in Graphene Devices. *Nat. Nanotechnol.* **2008**, *3*, 486–490.
19. Kim, K. S.; Zhao, Y.; Jang, H.; Lee, S. Y.; Kim, J. M.; Kim, K. S.; Ahn, J. H.; Kim, P.; Choi, J. Y.; *et al.* Large-Scale Pattern Growth of Graphene Films for Stretchable Transparent Electrodes. *Nature* **2009**, *457*, 706–710.
20. Jiang, D. E.; Cooper, V. R.; Dai, S. Porous Graphene as the Ultimate Membrane for Gas Separation. *Nano Lett.* **2009**, *9*, 4019–4024.
21. Kim, H. W.; Yoon, H. W.; Yoon, S.-M.; Yoo, B. M.; Ahn, B. K.; Cho, Y. H.; Shin, H. J.; Yang, H.; Paik, U.; *et al.* Selective Gas Transport through Few-Layered Graphene and Graphene Oxide Membranes. *Science* **2013**, *342*, 91–95.
22. O'Hern, S. C.; Boutilier, M. S.; Idrobo, J.-C.; Song, Y.; Kong, J.; Laoui, T.; Atieh, M.; Karnik, R. Selective Ionic Transport through Tunable Subnanometer Pores in Single-Layer Graphene Membranes. *Nano Lett.* **2014**, *14*, 1234–1241.
23. O'Hern, S. C.; Stewart, C. A.; Boutilier, M. S.; Idrobo, J.-C.; Bhaviripudi, S.; Das, S. K.; Kong, J.; Laoui, T.; Atieh, M.; *et al.* Selective Molecular Transport through Intrinsic Defects in a Single Layer of Cvd Graphene. *ACS Nano* **2012**, *6*, 10130–10138.
24. Iijima, S.; Yudasaka, M.; Yamada, R.; Bandow, S.; Suenaga, K.; Kokai, F.; Takahashi, K. Nano-Aggregates of Single-Walled Graphitic Carbon Nano-Horns. *Chem. Phys. Lett.* **1999**, *309*, 165–170.
25. Ohba, T.; Kanoh, H.; Yudasaka, M.; Iijima, S.; Kaneko, K. Quasi One-Dimensional Nanopores in Single-Wall Carbon Nanohorn Colloids Using Grand Canonical Monte Carlo Simulation Aided Adsorption Technique. *J. Phys. Chem. B* **2005**, *109*, 8659–8662.
26. Ohba, T.; Murata, K.; Kaneko, K.; Steele, W.; Kokai, F.; Takahashi, K.; Kasuya, D.; Yudasaka, M.; Iijima, S. $N_2$ Adsorption in an Internal Nanopore Space of Single-Walled Carbon Nanohorn: Gcmc Simulation and Experiment. *Nano Lett.* **2001**, *1*, 371–373.
27. Ohba, T.; Kanoh, H.; Kaneko, K. Superuniform Molecular Nanogate Fabrication on Graphene Sheets of Single Wall Carbon Nanohorns for Selective Molecular Separation of $CO_2$ and $CH_4$. *Chem. Lett.* **2011**, *40*, 1089–1091.
28. Rafati, A. A.; Hashemianzadeh, S. M.; Nojini, Z. B.; Naghshineh, N. Canonical Monte Carlo Simulation of Adsorption of $O_2$ and $N_2$ Mixture on Single Walled Carbon Nanotube at Different Temperatures and Pressures. *J. Comput. Chem.* **2010**, *31*, 1443–1449.
29. Makrodimitris, K.; Papadopoulos, G. K.; Theodorou, D. N. Prediction of Permeation Properties of $CO_2$ and $N_2$ through Silicalite *via* Molecular Simulations. *J. Phys. Chem. B* **2001**, *105*, 777–788.
30. Poling, B. E.; Prausnitz, J. M.; John Paul, O. C.; Reid, R. C. *The Properties of Gases and Liquids*; McGraw-Hill: New York, 2001; Vol. 5.
31. Steele, W. A. The Physical Interaction of Gases with Crystalline Solids. *Surf. Sci.* **1973**, *36*, 317–352.